Journal of Thermal Analysis, Vol. 54 (1998) 545-563

A DETAILED COMPARISON OF FIRST ORDER TRANSITIONS BY DSC AND TMC*

*A. Boller, M. Ribeiro*** and *B. Wunderlich*

Department of Chemistry, The University of Tennessee, Knoxville, TN 37996-1600; and Chemical and Analytical Sciences Division, Oak Ridge National Laboratory, Oak Ridge TN 37831-6197, USA

Abstract

Indium was analyzed with both, standard differential scanning calorimetry (DSC) and temperature-modulated DSC (TMDSC) using sinusoidal and saw-tooth modulation. Instrument and sample effects were separated during nucleated, reversible melting and crystallization transitions, and irreversible crystallization with supercooling. The changes in heat flow, time, and sample and reference temperatures were correlated as functions of heating rate, mass, and modulation parameters. The transitions involve three regions of steady state (an initial and a final region before and after melting/crystallization, a region while melting/crystallization is in progress) and one region of approach to steady state (melting peak to final steady state region). Analyses in the time domain show promise when instrument lags, known from DSC, are used for correction of TMDSC. A new method of integral analysis is introduced for quantitative analysis even when irreversible processes occur in addition to reversible transitions. The information was derived from heat-flux calorimeters with control at the heater block or at the reference temperature sensor.

Keywords: frequency domain, heat-flux calorimeter, indium, integral analysis, melting transition, pseudo-isothermal analysis, quasi-isothermal measurement, reversible melting, saw-tooth modulation, sinusoidal modulation, temperature-modulated calorimetry, time-domain

Introduction

The temperature calibration of a differential scanning calorimeter (DSC) relies on the analysis of sharp first-order transitions. On heating, indium and other suitable metals, as well as small-molecule crystals, can be used for such calibrations [1–6]. On cooling, melts supercool before crystallization because of the

---

* Presented in part at the 25th North American Thermal Analysis Conference, McLean, VA, USA, Sept. 7–9, 1997, Proceedings pgs. 706–713, R. J. Morgan, ed.

**Present address: Laboratoire de Thermodynamique et Génie Chimique, UPRES A CNRS, 6003, Université Blaise Pascal, F 63177 Aubière, France.

1418–2874/98/ $ 5.00

Akadémiai Kiadó, Budapest
Kluwer Academic Publishers, Dordrecht

need to nucleate, and one often uses the reversible isotropization of liquid crystals for calibration [7–11]. For macromolecules, crystallization involves molecular nucleation in addition to crystal nucleation [12]. The heating- and cooling-rate dependence of recordings of these melting and isotropization transitions has been used to determine calibration equations and to correct for instrument lags in standard DSC [11, 13]. The instrument lag is caused by the temperature gradient between sample and temperature sensor. It is customary to extrapolate the leading edge of the transition peak to the base-line caused by the heat capacity, or even better, to the base-line defined by zero heat-flow in the asymmetry-corrected DSC. The onset temperatures of melting and crystallization of In will be compared in this paper to other characteristic transition temperatures. It will be shown that a detailed check of the performance of calorimetry is possible by inspection of all temperature, time, and heat-flow signals when considering the construction features of the instrument.

The new temperature-modulated DSC (TMDSC) is in need of further investigation due to the periodically changing heating rates, going in many cases from heating to cooling. This is of importance, particularly after it could be verified with TMDSC that polymer melting is, indeed, irreversible [14], as suggested by earlier experimentation [12], and that irreversible melting effects can be linked to the crystal morphology [15] and time effects due to crystallization, reorganization, and melting [16–18]. It will be shown that TMDSC can use the same calibration as standard DSC when the data are analyzed in the time domain, using instantaneous heating and cooling rates $q(t)$. Problems arise when the different areas of steady state and approach to steady state, described next, overlap within the modulation cycles [19]. Furthermore, it will be shown that the methods developed to separate reversing and non-reversing effects [20] cannot be applied when the reversing heat flow deviates significantly from a sinusoidal response.

The heat of transition of sharp melting transitions is analyzed by standard DSC using the 'base-line method' [1]. The steady state 'A' that is characteristic of the heat capacity of the crystals, is replaced during melting by steady state 'B' in which the sample temperature is constant at T_m, and the reference temperature of the calorimeter continues to increase with time (Fig. 2, below). When the peak in temperature-difference (ΔT, proportional to heat flow, HF) is reached at the end of melting, a time period 'C' of renewed exponential approach to steady state occurs until a new steady-state base-line 'D', similar to 'A', is reached which is now characteristic of the heat capacity of the liquid. In heat-flux calorimetry, the sum of the heat-flux areas B and C above a base-line, defined by a proper apportionment between A and D, accounts for the heat of fusion. The progress of melting (at constant temperature) can be derived from the developing area B [1, 18]. This base-line analysis will be done by DSC and extended to time-domain studies of TMDSC.

A check of the melting and crystallization of In by TMDSC was made earlier using the Modulated DSC, MDSC™ of TA Instruments in which the sample-temperature sensor controls the temperature modulation [18]. In these experi-

ments the MDSC™ response is to increase the heating rate at the block to compensate for the larger heat flow needed for the transition. Although this shortens the time for transition, it forces the sample-temperature sensor to follow the modulation instead of recording the actual temperature of the sample. It was found that for an underlying heating rate of 0.2 K min^{-1} and a modulation amplitude of 0.5–1.5 K at periods of 60–90 s, the averages of the extrapolated onsets of melting and crystallization were within 0.1 K of the known melting temperature of indium when crystal nuclei were left after melting for subsequent crystallization [18]. The often given recommendation for quantitative analysis to cover the transition range with 5–6 periods of modulation can obviously not be fulfilled with such sharp-melting substances. This has led to the insinuation that TMDSC can give little information for first-order transitions. It will be shown in the following that the information gained from TMDSC studies can not only duplicate standard DSC, but also develop new fields of analysis [13–18].

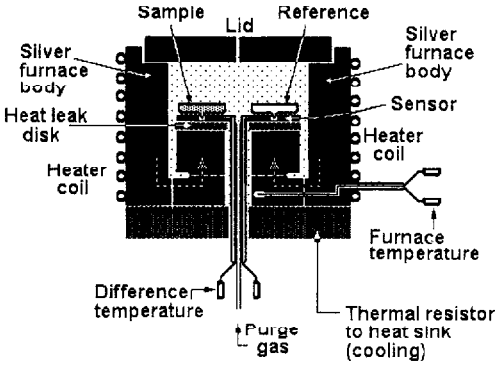

Fig. 1 Schematic drawing of the Mettler-Toledo DSC furnace

To better control steady state, a Mettler-Toledo Alternating DSC, ADSC™ 820, as shown schematically in Fig. 1, was chosen. Its modulation is controlled at a position far from the sample. Similar results can be obtained from the MDSC™, controlled at the reference temperature instead, as in the normal operation, at the sample temperature. This can easily be achieved by switching sample and reference. The observed effects are also evident in the power-compensated Perkin-Elmer Dynamic DSC, DDSC™, but need to be separately analyzed with full cognisance of the changed modulation and control mechanism relative to the heat-flux calorimeters. Standard DSC, sinusoidal modulation, and saw-tooth modulation have been done with the same calorimeter.

Experimental

In the Mettler-Toledo DSC 820 the modulation is little affected by fusion in the sample pan since the controlled variable is the furnace temperature, as seen

in Fig. 1. The reference temperature, T_r, is calibrated in reference to the furnace temperature, T_b, and the temperature difference, ΔT ($-T_r-T_s$), is determined by the sensor plates with multiple-junction thermocouples. Dry nitrogen gas with a flow rate of 10 ml min^{-1} was purged through the cell. The cell base was purged with N_2 at 150 ml min^{-1}. The gas flow rates were monitored and adjusted with a gas controller. The samples were weighed on a Cahn C-33 electro-balance to an accuracy of ±0.001% of the total load (50 mg).

Temperature calibration in the DSC mode was done with In (429.75 K), naphthalene (353.42 K), *n*-octane (116.4 K), acetone (177.9 K), cyclohexane (s/s 186.09 and s/l 297.7 K), cycloheptane (265.1 K), and Sn (505.05 K). The onsets of melting were determined by extrapolation of the melting peaks to the baseline. The samples were encapsulated in 40 μL standard aluminium crucibles without center pin and with a cold welded cover lid. Sample masses were varied from 49 μg to 19 mg. The reference pan was the same for all measurements.

The following experiments were carried out:

1) Linear heating and cooling with variable sample masses and heating rates (standard DSC).

2) Sinusoidal TMDSC with modulation amplitude A=1.5 K, period p=90 s and an underlying heating rate $\langle q \rangle$=1.0 K min^{-1} with 5.871 mg In to demonstrate complete melting and crystallization within separate cycles. This modulation option is not available at present for the commercial ADSC which uses a saw-tooth modulation.

3) Saw-tooth modulation with heating and cooling rates of 2 K min^{-1}, forcing an underlying heating rate $\langle q \rangle$ of 0.29 K min^{-1} by heating periods of 2 min, followed by cooling for 1.5 min. The operation of temperature-modulated calorimeters as well as the data treatment are discussed in the following references: DSC [1, 2], and TMDSC [2, 19–21].

Results and discussion

Standard DSC

In standard heat-flux DSC the temperature at the furnace is raised linearly with a selected heating rate q. The resulting temperature changes are shown in Fig. 2 for a heating rate of 10 K min^{-1}. When steady state is reached in the system, all points increase in temperature with close to the same heating rate. Unavoidable differences in heating rate arise from changes in heat capacity with temperature. After correction for asymmetries in the calorimeter, the temperature difference, ΔT, is proportional to the heat capacity difference between sample and reference (regions A and D) [1]. This ΔT is recorded as a function of time, and in Fig. 2 displayed as heat flow, HF in mW or mJ s^{-1}, *vs.* reference temperature, T_r, sample temperature, T_s, and time, t.

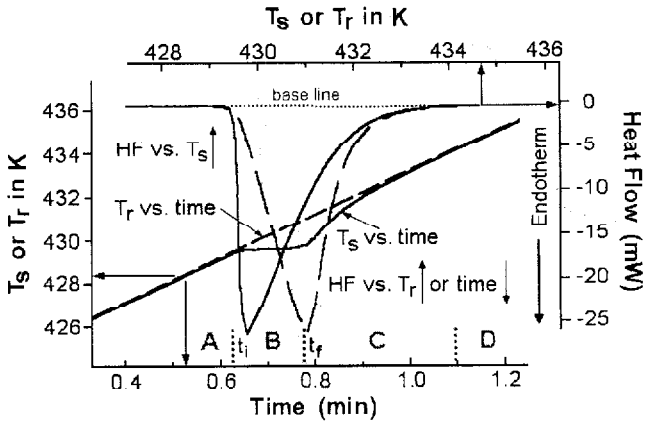

Fig. 2 Plot of heat flow (ΔT) and temperatures (T_r and T_s) *vs.* temperatures and time for indium. Standard DSC at a heating rate of 10 K min^{-1}. The different regions of melting are drawn for the recording *vs.* reference temperature or time

The transition of In occurs in region B of Fig. 2. Since In is a sharply melting substance of high melting rate [22], T_s is constant at T_m while T_r continues to increase linearly with rate q. The heat flow HF ($\propto\Delta T$) plotted *vs.* t or T_r increases thus also with a slope equal to q as long as the new steady state is maintained (10 K min^{-1}). The sharpness of the beginning and end of region B for In is a measure of the time for response of the calorimeter for the given heat flow (and sample heat conductivity). Broader melting substances can be judged against this calibration standard. The heat flow plotted *vs.* T_s should increase vertically during melting, indicating the constant sample temperature, making easy to detect deviations from steady state in B from the T_s recording.

In region C of Fig. 2 the sample temperature approaches exponentially the steady state of region D. In regions A and D the sample temperature lags slightly behind the reference, allowing calculation of the heat capacity C_s from ΔT ($\approx C_s q/K$, where K is the Newton's law calibration constant [1, 21]). Throughout the melting range the heat capacity of In is practically constant, giving a practically horizontal base-line. Note that a small correction is necessary for the ΔT-to-heat-capacity conversion if the base-line is not horizontal [1, 2].

To extract melting and crystallization temperatures in standard DSC, one finds the onset temperature at the intersection of the extrapolated base-line before the transition and the linear, low-temperature side of the peak [1]. A more precise 'zero onset' can be defined using the zero heat flow base-line. The zero heat-flow base-line is the asymmetry-corrected isotherm at the given temperature. With small samples (and/or low heating rates) the observed ΔT is sufficiently small in regions A and D to make the difference between the two onset temperatures negligible (Fig. 2).

The heat of fusion is, as indicated in the Introduction, proportional to the area of the melting peak of *HF* or ΔT *vs.* time or T_r over the regions B and C above a base-line defined by regions A and D. A detailed derivation of this co-called 'base-line method' can be found, for example, in reference [1]. Since $\Delta T(t)$ permits the transformation of the T_s scale to T_r or time, and is also a measure of the heat-flow amplitude, the two peak areas in Fig. 2 are equal. The integral of $\Delta T(t)$ over T_r or time in region B $[=q(t_f-t_i)^2]$ is equal to the difference between the integrals of the return to equilibrium from the peaks of $\Delta T(t)$ *vs.* T_s and T_r.

The effect of sample mass on the melting peak of In is shown in Fig. 3 for DSC at 5 K min^{-1}. The constant melting temperature is reached by T_s under the given conditions only from 0.049–5 mg. The onset and peak temperatures agree in this mass-range within 0.3 K. The remaining difference is due to a small temperature gradient between sensor and sample and seems unavoidable, even for small masses (see also [11]). For the 19 mg sample the recorded T_s shows a steady increase during melting, proof of a significant temperature gradient between sensor and sample. The slope of the melting peak is in this case only 3.9 K min^{-1} instead of the expected 5.0 K min^{-1}. This means that the sensor temperature increases in this case at a rate of 1.1 K min^{-1} during melting. The time to regain steady state after melting is approximately the same for the three smallest samples. For the 5 and 19 mg samples, it is much longer. The base-line method for the heat of fusion applies as before since the actual heat flow into the sample is governed largely by the sample-sensor temperature, not the actual sample temperature. The slower increase in ΔT is compensated since the heat of fusion is absorbed over a longer time. For smaller masses, the heat of fusion measurement is less precise due to the smaller area when plotting *HF* in W instead of W g^{-1}. For larger masses, the base-line may become uncertain because of the wider melting range.

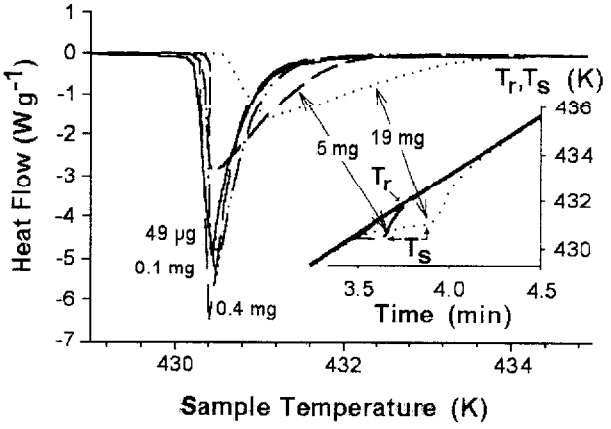

Fig. 3 Mass dependence of the melting of indium. Standard DSC at a heating rate of 5.0 K min^{-1}

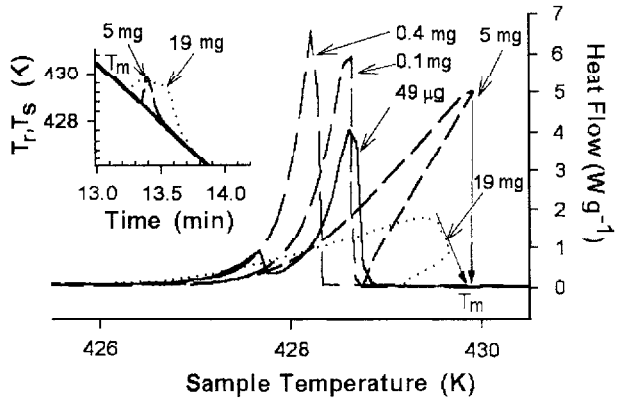

Fig. 4 Mass dependence of the crystallization of indium. Standard DSC at a cooling rate of 5.0 K min^{-1}

Temperature calibration on cooling can normally not be done with In by using the onset temperatures of crystallization because of supercooling due to the need of crystal nucleation. Once crystallization is nucleated, however, the exothermic heat of crystallization may heat the sample to the equilibrium melting temperature. For In, supercoolings of 1 to 1.5 K are typical [13]. Figure 4 illustrates the crystallization of In at a cooling rate of 5 K min^{-1} for the same samples as in Fig. 3. Although the onset temperatures are far from the equilibrium and not reproducible due to the variation in nucleation, one can see in Fig. 4 that a sample of about 5 mg In has a heat of crystallization just big enough to increase the sample temperature to 429.9 K, the equilibrium melting temperature as determined in this set of experiments. The literature melting temperature is 429.75 K. The difference of 0.15 K is the correction that must be applied to all measurements in this paper. For the largest mass of 19 mg the sample temperature is almost constant during much of the crystallization, but due to the temperature gradient between sample and sensor, which is, as on heating, a function of the temperature difference between furnace and sample, the sensor temperature shows a linear decrease with time. The cooling rate of the sensor temperature is, as on heating, about 1 K min^{-1}. This steady state *HF* during crystallization can be extrapolated to zero *HF* and one reaches again 429.9 K, as expected. The double-peak of the smallest sample may be due to an uneven sample distribution within the pan. This sample is so minute that a major portion may not have contacted the bottom of the pan.

Sinusoidal TMDSC

Single melting peak

Figure 5 illustrates the sinusoidal temperature modulation at a sufficiently fast underlying heating rate <*q*> so that only one melting occurs. The extrapo-

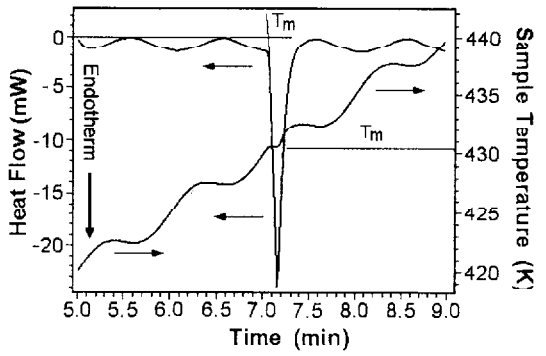

Fig. 5 Single melting peak of 5.87 mg of indium on TMDSC at an underlying heating rate <q> of 5.0 K min^{-1}. Modulation parameters: A=1.0 K, p=60 s. Peak temperature at 430.5 K, onset of melting at $q(t)$=11 K min^{-1}

lated onset of melting is close to the maximum heating rate ($2\pi\omega$+<q>) and indicates 430.5 K, as one would expect for an 11 K min^{-1} heating rate [11, 13]. Overall, the curve corresponds closely to standard DSC and when analyzed in the time domain, as shown in Fig. 5, the only difference is in the sinusoidal base-line that may take a greater effort to generate. Note, that the sample temperature has a horizontal portion of constant T_s, as also seen in the standard DSC trace of Fig. 2. The extrapolated peak temperature, obtained by linear extension of the two sides of the peak, is 430.55 K, indicating the close to vertical increase of heat flow when plotted *vs.* T_s. No advantage can be gained in such analysis by TMDSC over DSC.

Two melting peaks

Two melting peaks and one crystallization are produced in Fig. 6 from an experiment where <q> was lowered to 1.0 K min^{-1} and A and p were increased to 1.5 K and 90 s, respectively. The melting and intervening crystallization peaks are well separated and steady states are reached between the three transitions. During the first melting, marked in the figure by the letter A, the temperature of the sample drops slightly after the onset of melting at 430.3 K to a temperature of 430.2 K. Since the first melting was complete, as judged from the heat of fusion, it causes the sample to supercool in the subsequent half-cycle for crystallization, marked B. The onset temperature of crystallization B is 428.9 K, a supercooling of 1.2 K. Only when the melting is incomplete can crystallization occur without supercooling [13]. The peak temperature in the crystallization, however, reaches 430.1 K, which is within 0.1 K of the minimum T_s in the first melting (sensor temperature). In this case of supercooling before crystallization it would be inaccurate to use the onset temperature for calibration. Only the peak temperature can be used to fix the equilibrium temperature of the transition after one has

made certain that sufficient heat of crystallization was generated to raise the sensor temperature to T_m, as shown in Fig. 4 for standard DSC.

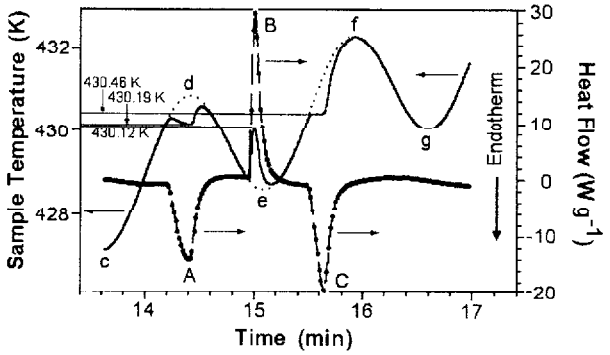

Fig. 6 Two melting peaks and one crystallization peak of 5.87 mg of indium on TMDSC at an underlying heating rate <q> of 1.0 K min^{-1}. The dotted lines mark the undistorted sinusoidal sample temperatures. Modulation parameters: A=1.5 K, p=90 s

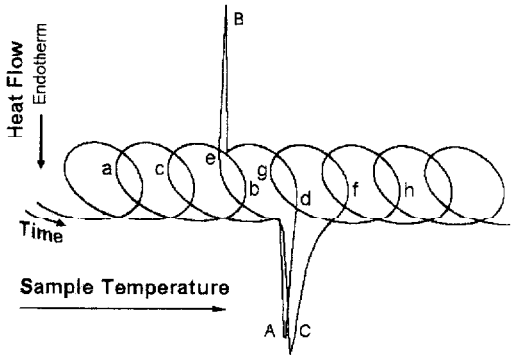

Fig. 7 Lissajous figure of the melting of indium as shown in Fig. 6 with the same markings

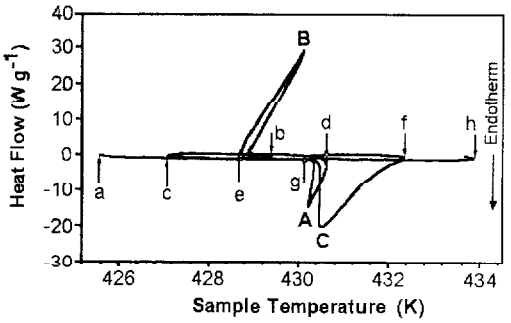

Fig. 8 Lissajous figure of the melting of indium as shown in Fig. 6 with the same markings, as in Fig. 7, but with changed scales for quantitative evaluation

The second, and last melting, C, occurs during the almost linear increase in the sinusoidal temperature program (at maximum heating rate, 7.3 K min^{-1}) The temperature of the isothermal segment shows a T_s of the sensor of 430.5 K, which indicates a (heating-rate dependent) increase of the sensor temperature of about 0.25 K, in agreement with the calibration by standard DSC [11, 13].

The integration of the heat flow for the individual melting and crystallization transitions in sinusoidal TMDSC is more difficult than the integration in standard DSC or saw-tooth TMDSC because a sinusoidal base-line has to be generated. Programs to do so have been developed in our laboratory [13, 23], but are not yet included in any of the commercial softwares.

The interpretation of TMDSC experiments is helped by inspecting Lissajous figures of the instantaneous heat flow, $HF(t)$, plotted against the corresponding sample temperature, $T_s(t)$, as shown in with different scales in Figs 7 and 8 for the same run as in Fig. 6. Additional modulation cycles before and after melting and crystallization are reproduced (a–b, g–h). The lower-case letters mark the minima and maxima of the sample temperature, the capical letters, the transition peaks. The letters in Figs 6–8 mark the same points of the experiment. Figure 7 is drawn to be able to follow the progress of the measurement, Fig. 8. more clearly reveals the temperature changes of the sample-temperature sensor. First melting starts with peak A (following point c), decreasing the sample temperature to 430.19 K (Fig. 6). The decrease in sensor temperature goes parallel with the decrease in heating rate to 0 K min^{-1} and the temperature lowering observed in Fig. 3. As melting is completed, steady state is approached again during segment d of the curve, and normal modulation resumes. With peak B, the crystallization starts and heats the sample (despite the cooling attempted by the modulation), reaching 430.12 K, close to the equilibrium melting temperature. This is quickly followed by segment e, that reestablishes steady state. Final melting occurs at peak C with a higher heating rate, now at an indicated temperature of 430.19 K. Segment f reestablishes steady state modulation.

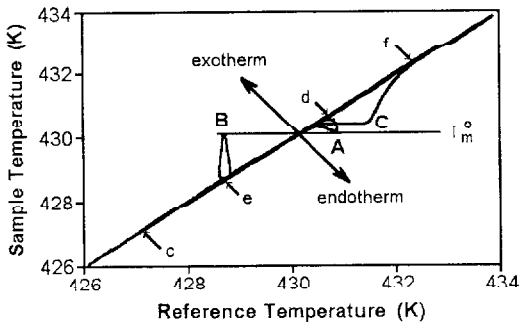

Fig. 9 Plot of sample temperature *vs.* reference temperature for the run of Fig. 6

A final display is given in Fig. 9. It shows the temperature changes of T_s *vs.* T_r for the run of Fig. 6. The events are labelled with the same lower-case and capital letters to show the correspondence to Figs 6–8. The exothermic and endothermic directions are also indicated. The fusion (A) is completed at close-to-zero heating rate, reaching the recovery of the melting temperature on crystallization (B). Both are marked as being close to the equilibrium melting temperature T_m°. The melting at faster heating (C) is clearly occurring at the higher sample sensor temperature.

This detailed study of TMDSC of a substance that is known to melt and crystallize fast shows that under properly chosen conditions the modulation does not change the behaviour of the scanning calorimetry. The key condition for the easy analysis is that steady state is recovered in every case before the reversal of the transition begins.

Seven melting peaks

Figures 10–13 repeat the prior analysis for an even slower underlying heating rate of 0.1 K min^{-1} so that seven melting and six recrystallization peaks can be observed. The modulation amplitude A and period p were also reduced to cause partial melting when initially reaching the melting temperature. Figure 10 reveals that the melting peaks numbered 1 to 6 are incomplete, i.e. after the temperature drops below the melting temperature, crystal nuclei remain. As a result, the corresponding crystallization peaks 1′ to 6′ are continuous with the completion of melting because sufficient nuclei are present to reverse the crystallization. Only after crystallization is completed is steady state regained. The cross-over from endothermic melting to exothermic crystallization occurs close to the equilibrium melting temperature T_m°. For peak 2 the enlarged Lissajous fig-

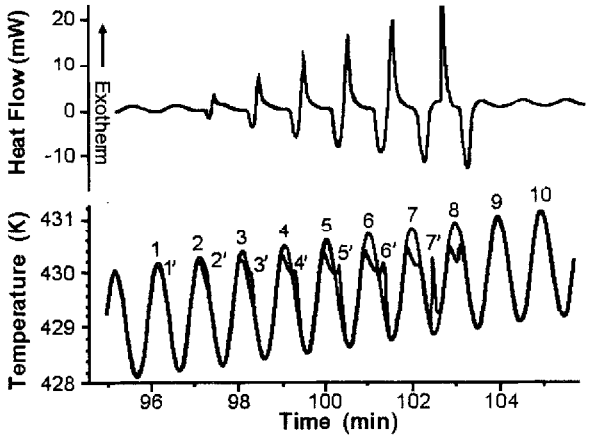

Fig. 10 Multiple melting peaks and crystallization peaks of 5.87 mg of indium on TMDSC at an underlying heating rate <q> of 0.1 K min^{-1}. The undistorted sinusoidal sample temperatures are also indicated. Modulation parameters: A=1.0 K, p=60 s

ure is given in Fig. 11. Figure 12 displays the temperature profile on close to complete melting and crystallization of peaks 6 and 6′.

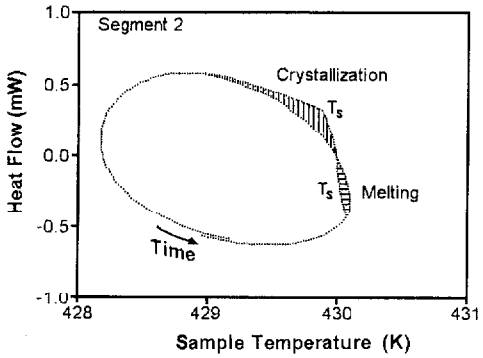

Fig. 11 Lissajous figure of segment 2 of the TMDSC of Fig. 10. The trace free of crystallization and melting effects was generated making use of the recorded reference temperature

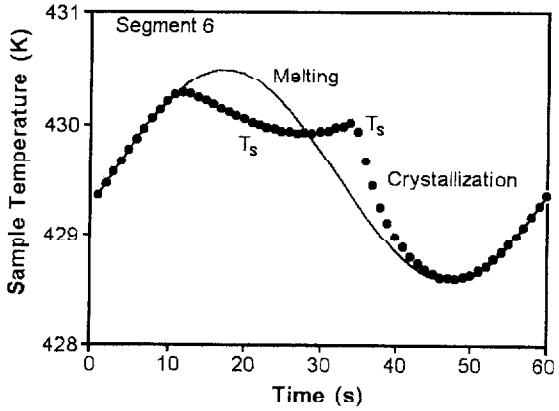

Fig. 12 Expanded plot of the sample temperature *vs.* time of segment 6 of the TMDSC of Fig. 10. The trace free of crystallization and melting effects was generated making use of the recorded reference temperature

To resolve the effect of partial melting and complete melting one can compare Figs 13 and 9. The peaks, 7, 8 and 7′ of Fig. 13 are analogous to A, C, and B of Fig. 9 and illustrate melting followed by supercooling during which steady state can be recovered and renewed crystallization with heating of the sample due to crystallization exotherm. The detailed shapes depend on the position in the modulation cycle (phase angle). Melting peaks 1 to 6, in contrast, change continuously from melting to crystallization with the crossover through ΔT=0 occurring close to T_m°. The final melting peak 8 in Fig. 13 is unique by going from a high heating rate at the beginning of melting which causes a lag in T_s of about 0.2 K through $q(t)$=0 to end at an equally high cooling rate and an advance in T_s

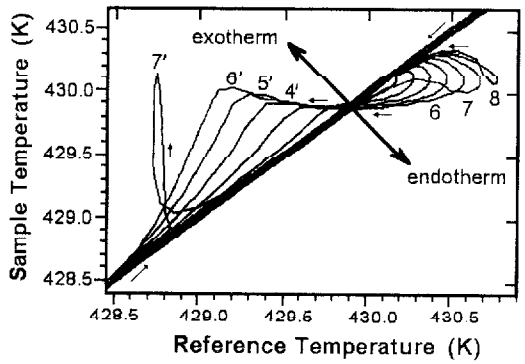

Fig. 13 Plot of sample temperature *vs.* reference temperature for the run of Fig. 10. Check Fig. 9 for study of the supercooling effect

of about 0.2 K, i.e. it leaves and enters the diagonal of $\Delta T \approx 0$ at the same T_s. Figure 13 illustrates that the position in the modulation cycle, its phase angle, is an important variable in the appearance of the melting and crystallization peaks. Using a quasi-isothermal analysis [24], any position along the changing phase angle can be frozen and analyzed as done before for the melting of In [13].

Integral analysis

A new type of analysis is illustrated in Fig. 14. It traces the change in enthalpy during modulation in the temperature region where continued melting and crystallization occurs. The upper curve gives an estimate of the enthalpy change as a function of sample temperature as one traverses the various melting and crystallization cycles of the experiment in Fig. 10. The lower curve represents the same as a function of time. The heat-flow curves $HF(t)$, were integrated to enthalpy after multiplication with the appropriate calibration constant [1, 2].

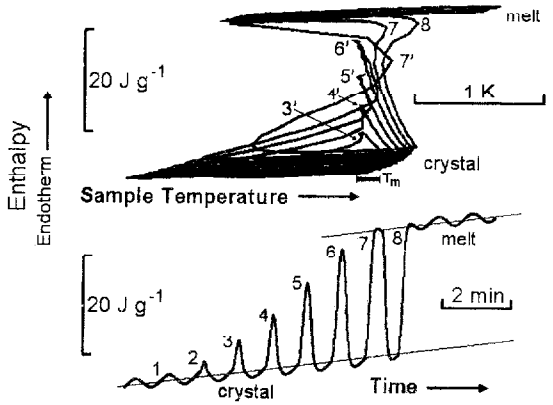

Fig. 14 Integral analysis of the enthalpy in the melting and crystallization region for the TMDSC run of Fig. 10

The upper curve of Fig. 14 shows particularly clearly on its lower right how the onset of melting, indicated by the sample-temperature sensor, is displaced continually to higher temperature as one goes from segment 3 to 8 (0.03 K for each increase in $q(t)$ by one K min^{-1} [13]). The increase in heating rate results from the 0.1 K earlier start per cycle of the melting due to the underlying heating rate. Assuming cycle 3 (Fig. 11) is at a heating rate of about $q(t)$=0.1 K min^{-1}, i.e. at the modulation maximum, cycle 6 (Fig. 12), in turn, is moved backwards by about 30° in phase angle, accounting for a heating rate of $q(t)$=3.2 K min^{-1} and about 0.1 K increase in onset temperature. Considering the uncertainty of the onset of melting at zero heating rate of ±0.1 K [11], places the equilibrium melting point in the marked region of Fig. 14 (compare also with Fig. 6). All deviations from vertical approaches between crystal and melt are due to instrument lag.

Even more interesting is the bottom plot of Fig. 14. It clearly reveals that melting of segments 1 to 6 does not reach the enthalpy of the melt. It also shows that approximate steady state crystals are reached on subsequent crystallizations 1′ to 6′ (bottom area of the curve). Melting 7 reaches a steady state melt for a short time (top area of the curve), then crystallizes (7′) to reach steady state crystals again, and finally, melts with segment 8 completely. The enthalpy peaks describe subsequent meltings and crystallizations. Although their exact shapes are distorted, mainly due to the overlap of the return to steady state from melting (region C, above, Fig. 2) with crystallization region, it is possible to approximate the progress of melting and crystallization. This type of analysis should be of use to follow the melting of macromolecules where crystallization is inhibited, but reorganization, crystal perfection and local recrystallization are common and the melting range is broad [12–18].

Reversing heat flow

The final point to be addressed is the question if the TMDSC traces in Figs 5, 6 and 10, which appear to be reversible can also be studied using the common Fourier transformation into the frequency domain. The analysis can be done, for example, by finding the modulation amplitudes of the observed heat flow, $<A_{HF}(t)>$, and sample temperature, $<A(t)>$, and deriving heat capacity from the ratio $<A_{HF}(t)>/(<A(t)>\omega)$. In this ratio $<A(t)>$ should also be equal to the temperature-modulation amplitude A, set at the beginning of the experiment, and ω is the modulation frequency ($=2\pi/p$) [20]. The analysis is usually carried out by finding the contributions of frequency ω to heat flow and sample temperature (the first harmonic) to the instantaneous heat flow $HT(t)$ and sample temperature $T_s(t)$. This is a pseudo-isothermal analysis and can make use of the same formalism [20] as for the quasi-isothermal method of measurement with $<q>=0$ [24]. This analysis is, however, only correct if the reversing calorimeter response to modulation is sinusoidal. Strictly this is true only if the sliding averages over one period p, $<HF(t)>$, the total heat flow, and $<T_s(t)>$, the average temperature, are

constant over two, or better three modulation cycles. In this case the Lissajous figure as in Figs 7 and 11 are ellipses when corrected for the underlying temperature increase (by subtraction of $<q>t$ or plotting *vs.* dT_s/dt). In the melting region of In this is obviously not the case.

Figure 15 shows the actual heat-flow plot of Fig. 10 [$HF(t)$] and the derived total heat flow $<HF(t)>$ which involves averaging over one modulation cycle, and the 'reversing heat-flow amplitude' which involves for its calculation averaging of some components over two modulation cycles [20]. The deviations of $<A(t)>$, obvious from Fig. 10, are much smaller. Neither the peak positions, nor the amplitudes have any easily discernible relation to the actual data. Note, that even the total heat flow is quite different from the HF of standard DSC, which it is often assumed to be equal to (compare with Fig. 2). Figure 16 shows a com-

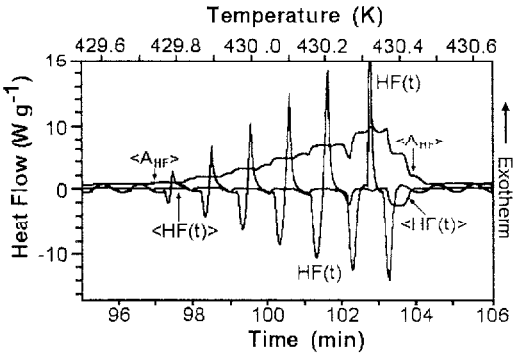

Fig. 15 First harmonic contribution to the heat flow amplitude $<A_{HF}>$ of the Fourier transformation of $HF(t)$ of the data of Fig. 10. Also shown is the total heat flow $<HF(t)>$ that is often considered equal to the standard DSC heat flow as in Fig. 2

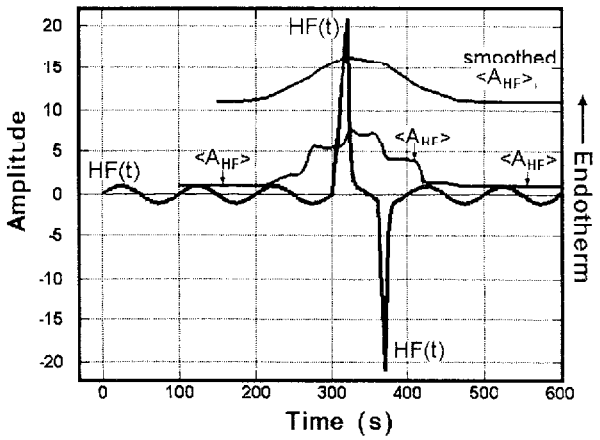

Fig. 16 Model calculation of a single melting, followed by crystallization using the software generated in ref. [21] and available through [2]. Parameters p=100 s, arbitrary units of amplitudes of modulation and melting and crystallization peaks

parison to a modeling of melting [18], done with a simple spread-sheet program, available through our WWW site [2]. The appearance of $<A_{HF}(t)>$ is quite similar to the last modulation cycle with crystallization and melting in Fig. 15 (7', 8). The smoothed $<A_{HF}(t)>$ is the output of the common commercial software [20]. It uses elements of three modulation cycles and is even further removed from giving a realistic picture of the actual reversible crystallization and melting.

Saw-tooth TMDSC

A saw-tooth modulation is often available as an option for modulation. Figure 17 illustrates conditions that lead to three melting steps, separated by two crystallizations. The figure shows elements of both, the standard DSC (B, C, E) and the changes in heating rate of TMDSC (A, D). The transitions B, C, and E are easily analyzed as outlined in the Section of Standard DSC. For A and D the abrupt change from heating to cooling and vice versa need to be considered as in the Section of Sinusoidal TMDSC.

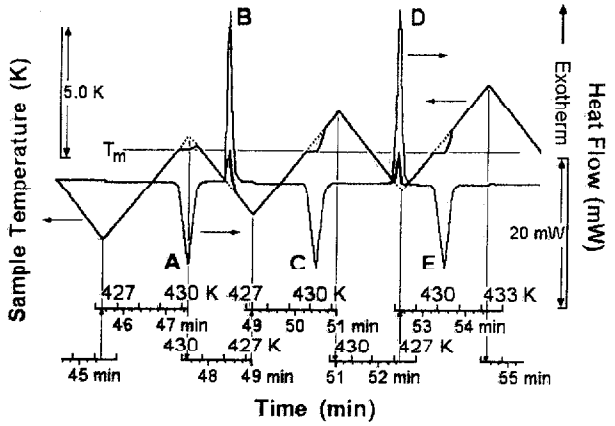

Fig. 17 Saw-tooth modulation for TMDSC showing the melting of In, similar to Fig. 6. The abscissa shows a continuous time scale and an interrupted reference-temperature scale which follows the saw-tooth modulation. Heating and cooling segments of 2.0 K min^{-1}, two minute heating segments, followed by 1.5 min cooling to give an underlying heating rate of 0.29 K min^{-1}

The analysis of the saw-tooth experiment in the time-domain is possible, as shown above. One advantage over sinusoidal modulation is that the four regions of melting and crystallization are easily identified and the detection of steady state is elementary. At steady state the temperature increases linearly and the heat-flow response is horizontal for strict steady state or changing slightly in case the heat capacity is temperature dependent. As mentioned in the Section of Standard DSC, in the latter case a correction of the quantitative analysis of DSC is needed because of the difference in heating rate of reference and sample temperature [1, 2].

The analysis in the frequency domain is even harder than in the case of sinusoidal modulation. The description of a saw-tooth in itself needs to consider already many higher harmonics.

Conclusions

Indium is an ideal calibration substance because of its sharp and rapid melting and fast crystallization after nucleation (no superheating, easy availability of pure samples, quick crystallization to sufficiently perfect crystals, and relatively small supercooling (1–1.5 K)). It can be used for calibration of both, DSC and TMDSC. The onset of melting and crystallization of In in standard DSC experiments needs to be corrected for heating and cooling rates because of a temperature gradient between sample and temperature sensor in regions A and D, delineated in Fig. 2 (lag≈0.03×q [11]). During melting (region B), the temperature of In is largely constant. On cooling with sufficient sample mass, the sample temperature rises up to the melting temperature and can also be used to calibrate the calorimeter (Fig. 4). With sufficient mass of In, the sensor temperature shows a small increase during melting after reaching the equilibrium temperature of the transition (Fig. 3) and decrease during crystallization (Fig. 4, ≈1 K min^{-1} in both cases). The cause is the changing temperature gradient between sample and sensor.

Temperature-modulated DSC shows quantitatively the same effects when analyzed in the time domain and if the melting and crystallization peaks are sufficiently separated to in-between achieve steady state (Figs 5–9). The need to develop a sinusoidal base-line makes the evaluation of heats of transition more cumbersome than standard DSC. Lissajous figures (Figs 7 and 8) help in the analysis, and a plot of T_s *vs.* T_r (Fig. 9) permits to check in one experiment the various kinetics effects (lag of T_s with heating rate and change of the temperature gradient between sample and sensor on melting and crystallization). On choosing the modulation parameters so that melting is incomplete when the temperature drops below the melting temperature, the reversible melting of In can be studied (Fig. 10). The Lissajous figures reveal that the cross-over from melting to crystallization occurs close to the equilibrium melting temperature (Figs 11 and 12). The plot of T_s *vs.* T_r (Fig. 13) is largely different for incomplete and complete melting. A new integral analysis results in plots of the change of enthalpy with sample temperature or time (Fig. 14). It indicates the progress of partial melting and may become an important tool to follow irreversible processes in broad melting ranges, such as in the melting of semicrystalline macromolecules.

Attempts to analyze the melting in the frequency domain by evaluation of the amplitude (or phase shift) of the reversing heat flow of the first harmonic of a Fourier transformation leads to little useful information (Figs 15 and 16). Higher harmonics are necessary to properly reproduce the heat-flow shape, even in reversible melting. It is noteworthy that the total heat flow calculated in such fashion is also not representing the actual heat flow necessary for fusion since it retains all higher harmonic terms of the reversible melting as shown in Fig. 15.

The melting and crystallization during a saw-tooth TMDSC are segments of a series of standard DSC experiments (Fig. 17). It is an advantageous method of analysis of the easy recognition of steady state and its loss. The change of heating to cooling during incomplete melting is a possible method to determine the melting temperature of a pure, sharp melting substance and calibrate the TMDSC on cooling. It avoids the use of fully reversible transitions of liquid crystals.

All three methods of DSC, standard (Fig. 2), sinusoidal modulation (Fig. 10), and saw-tooth modulation (Fig. 11) have advantages for special applications in the analysis of melting and crystallization transition. The analysis of In can serve as a proving ground of the equipment on hand and be used for fine tuning and calibration. The thermal analysis of materials may require in different situation a different DSC method.

* * *

This work was supported by the Division of Materials Research, National Science Foundation, Polymers Program, Grant # DMR-9703692 and the Division of Materials Sciences, Office of Basic Energy Sciences, US Department of Energy at Oak Ridge National Laboratory, managed by Lockheed Martin Energy Research Corp. for the US Department of Energy, under contract number DE AC05-96OR22464. Support for instrumentation came from TA Instruments, Inc. and Mettler-Toledo Inc. Research support was also given by ICI Paints.

References

1 B. Wunderlich, 'Thermal Analysis', Boston: Academic Press, 1990.
2 B. Wunderlich, Computer assisted learning course: 'Thermal Analysis of Materials', Lect. 20 and 21, 1997 available at http://funnelweb.utcc.utk.edu/~athas.
3 G. W. H. Höhne, H. K. Cammenga and W. Eysel, Thermochim. Acta, 160 (1990) 1.
4 H. K. Cammenga, W. Eysel, E. Gmelin *et al.*, Thermochim. Acta, 219 (1993) 333.
5 G. W. H. Höhne, Thermochim. Acta, 69 (1983) 175.
6 G. W. H. Höhne and E. Glöggler, Thermochim. Acta, 151 (1989) 295.
7 G. W. H. Höhne, J. E. K. Schawe and C. Schick, Thermochim. Acta, 221 (1996) 129.
8 P. Skoglund and A. Fransson, Thermochim. Acta, 276 (1996) 27.
9 C. Schick and G. W. H. Höhne, Thermochim. Acta, 187 (1991) 351.
10 J. D. Menczel and T. M. Leslie, Thermochim. Acta, 166 (1990) 309.
11 W. Chen and B. Wunderlich, Proc. 25th NATAS Conf. in McLean, Va., Sept. 7–9, 1997, R. G. Morgan, ed., (1997) 637; to be published Thermochim. Acta, 1998.
12 B. Wunderlich, 'Macromolecular Physics, Volume 3: Crystal Melting'. Academic Press, New York 1980.
13 K. Ishikiriyama, A. Boller and B. Wunderlich, J. Thermal Anal., 50 (1997) 547.
14 K. Ishikiriyama and B. Wunderlich, Macromolecules, 30 (1977) 4126.
15 I. Okazaki and B. Wunderlich, Macromolecules, 30 (1997) 1758.
16 K. Ishikiriyama and B. Wunderlich, J. Polymer Sci., Part B: Polymer Phys., 35 (1997) 1877.
17 I. Okazaki and B. Wunderlich, Macromol. Chem. Phys., Rapid Commun., 18 (1997) 313.

18 B. Wunderlich, I. Okazaki, K. Ishikiriyama and A. Boller, Proc. 25th NATAS Conf. in McLean, Va., Sept., 7–9, 1997, R. G. Morgan, ed., 49; to be published, Thermochim. Acta, 1998.
19 B. Wunderlich, A. Boller, I. Okazaki and S. Kreitmeier, Thermochim. Acta, 282–283 (1996) 143.
20 B. Wunderlich, Y. Jin and A. Boller, Thermochim. Acta, 238 (1994) 277.
21 B. Wunderlich, J. Thermal Anal., 48 (1997) 207.
22 M. Jaffe and B. Wunderlich, Proc. 2nd ICTA. 'Thermal Analysis', Vol. 1, p. 387, E. F. Schwenker and P. D. Garn, eds., Academic Press, New York 1969.
23 B. Wunderlich, A. Boller, I. Okazaki and K. Ishikiriyama, Thermochim. Acta, 304-305 (1997) 125.
24 A. Boller, Y. Jin and B. Wunderlich, J. Thermal Anal., 42 (1994) 307.